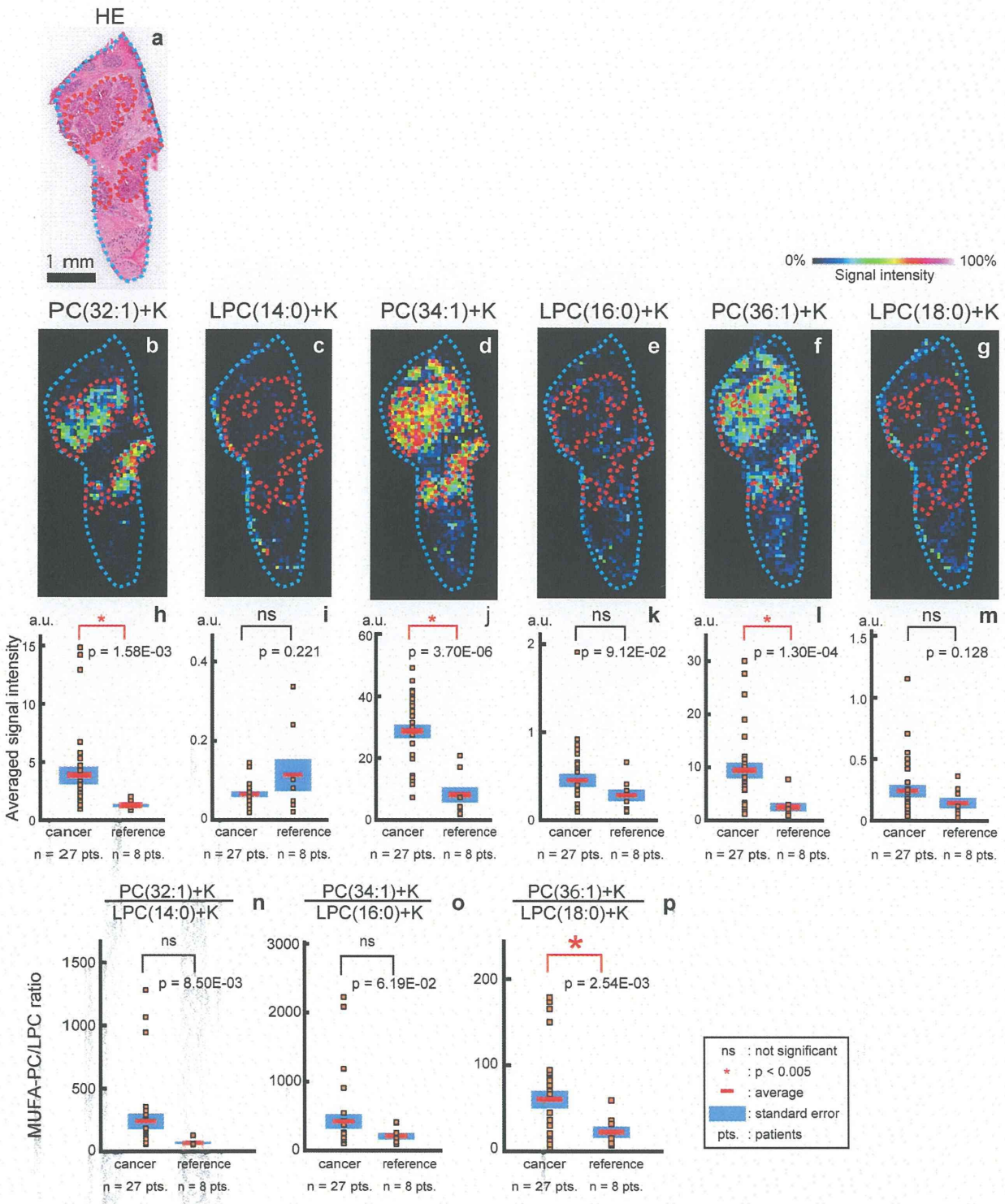

Figure 5. The ratios of MUFA-PCs to LPCs were significantly higher in cancerous areas than in reference areas. (a) The areas that are circled with red show the cancerous areas in the hematoxylin and eosin stained image. (b) A distribution image of PC(32:1)+K. (c) A distribution image of LPC(14:0)+K. (d) A distribution image of PC(34:1)+K. (e) A distribution image of LPC(16:0)+K. (f) A distribution image of PC(36:1)+K. (g) A distribution image of LPC(18:0)+K. (h) Plot of the intensities of PC(32:1)+K. (i) Plot of the intensities of LPC(14:0)+K. (j) Plot of the intensities of PC(34:1)+K. (k) Plot of the intensities of LPC(16:0)+K. (l) Plot of the intensities of PC(36:1)+K. (m) Plot of the intensities of LPC(18:0)+K in 35 ROIs. (n) Plot of the ratios of PC(32:1)+K to LPC(14:0)+K. (o) Plot of the ratios of PC(34:1)+K to LPC(16:0)+K. (p) Plot of the ratios of PC(36:1)+K to LPC(18:0)+K.
doi:10.1371/journal.pone.0061204.g005

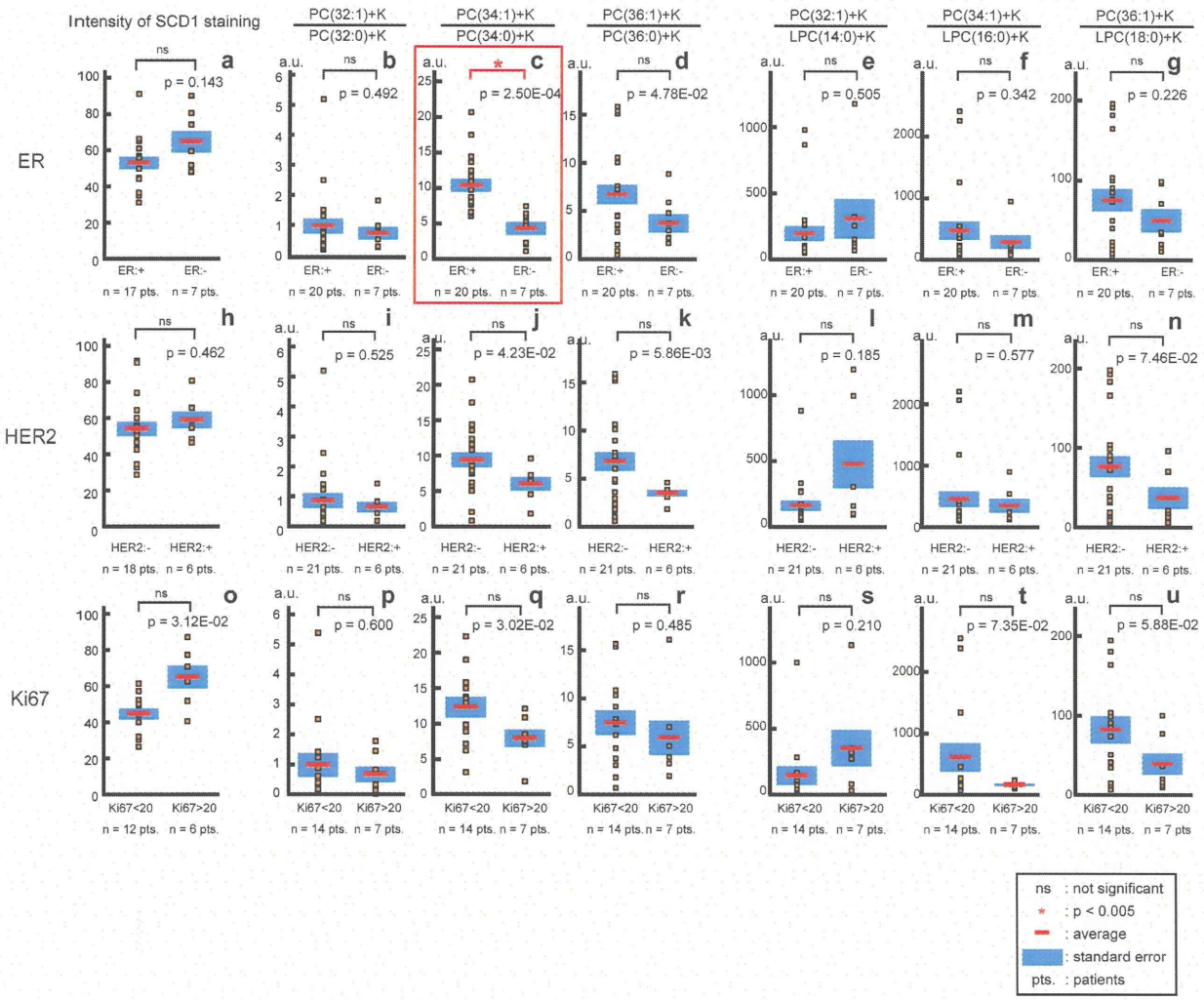

Figure 6. SCD1 expression and the ratios of MUFA-PCs to SFA-PCs and LPCs for differences in ER, HER2, and Ki67 expression. The intensities of SCD staining (a, h, o) and the ratios of MUFA-PC compared to SFA-PC (b–d, i–k, p–r) and LPC (e–g, l–n, s–u) were shown by the differences in ER (a–g), HER2 (h–n), and Ki67 (o–u). All of the cancer lesions were divided into two groups according to the differences in ER, HER2, and Ki67 expression and lesions with less aggressiveness are shown on the left side of each graph.
doi:10.1371/journal.pone.0061204.g006

a relatively high amount of MUFA-PCs. Among the 3 ratios of MUFA-PCs to SFA-PCs, only the ratio of PC(36:1) to PC(36:0) were found to be significantly related to the high SCD1 expression; this observation can be attributed to the SCD1 preferentially desaturating FA(18:0) over FA(16:0) [40]. The result that only the ratios of PC(36:1) to PC(36:0) in cancerous areas were higher might be explained by higher affinity of SCD1 to FA(18:0).

On the other hand, the result of a sub-analysis of the ratio of MUFA-PC [PC(34:1)] to SFA-PC [PC(34:0)] with respect to ER expression was not consistent with the SCD1 expression pattern: SCD1 expression did not show a significant difference between the ER positive groups and ER negative groups. This result could be explained by 2 possible reasons. First, there may be other factors that regulate the relative amount of MUFA-PCs. The LPCATs that catalyze the insertion of MUFAs into LPCs might be one of the candidates. [39,41]. We found from a microarray analysis that LPCAT3 is expressed at higher levels in ER positive tissues than in ER negative tissues [42,43], which is consistent with the correlation between ER status and the MUFA-PC/SFA-PC ratio that was observed in the present study. LPCAT4 is one LPCAT isoform that shows a higher specificity to FA(18:1) [44]. LPCAT4 may be acting as a regulating factor in this study as well, although no comparative studies on LPCAT4 expression between ER-positive and ER-negative breast cancer lesions have been reported. Second, a greater activity of the SCD1 enzyme in ER-positive cells than that in ER-negative cells could cause an excessive production of MUFA-PCs in these cells. As the endogenous mechanisms to regulate the enzymatic activity of SCD1 are poorly understood, further studies on the SCD1 activity and its regulatory mechanism might be warranted.

We alternatively defined tumor aggressiveness on the basis of immunohistochemical staining of pathological markers, ER negativity, HER2 positivity, and high Ki67 expression. Because exogenous HER2 overexpression induces upregulation of fatty acid synthase (FASN) in breast cancer cells, the pathway involving the HER2 receptor is generally considered to regulate lipogenic

enzymes [45]. The activation of lipid metabolism in tumor cell proliferation is widely accepted [2,3]; thus, the correlation of Ki67 expression level and PC compositions were expected. However, the ratios presented in Figure 6 did not show significant differences between high- and low-expression groups of HER2 and Ki67. We therefore could not prove the effect of the expression of these molecules on the acyl chains in PCs. Regarding the result that only the ratio of PC(34:1)/PC(34:0) showed significant differences between ER-positive and ER-negative groups, we propose the following mechanism. SCD1 predominantly converts FA(18:0) to FA(18:1) [40] and LPCATs combine FA(18:1) and LPC(16:0) [44], putatively the most abundant LPC, [46,47] to generate PC(34:1). Therefore, PC(34:1) might be preferentially affected by the alteration of expression and activity of the enzymes. However, further studies on this mechanism are warranted to confirm these statements that are based on propositions.

In this study, we analyzed the PCs of specific carbon chain lengths and saturation to characterize the specimens. Since polyunsaturated fatty acids have been argued to function in cancer hallmarks by maintaining and disrupting membrane microstructures and by tuning signal transductions [48,49], further studies involving PCs that are composed of fatty acids with longer chains and greater degrees of unsaturation might lead to a better understanding of the function of phospholipids in cancer pathogenesis.

Currently, MALDI-IMS as a technique is developing and is expected to have enough resolution to allow investigators to define and analyze smaller areas. If MALDI-IMS could be improved, it would be a useful tool for exploring the mechanisms of carcinogenesis and cancer metastasis. The analysis of cancer stem cells like treatment-resistant breast cancer cells that share small populations of thousands of cells in lesions [50] might be possible. A combination of improved MALDI-IMS and immunohistochemical staining might reveal a correlation between lipid composition and receptor expression, which has been scarcely reported [51]. MALDI-IMS has the potential to be a favorable tool to study breast cancer tissues with molecular heterogeneity [52]. We are attempting to improve the capabilities of MALDI-IMS by adopting new agents as a matrix [53], by using mass microscopes [54] and so on to perform these analyses in the near future.

Conclusions

IMS was used to successfully visualize molecular species of PCs and LPCs in human breast cancer tissue specimens. Some MUFA-PCs and SFA-PCs [PC(32:1), PC(34:1), PC(36:1), and PC(34:0)] were relatively localized in cancerous areas rather than the rest of the sections, while LPCs were equally distributed. Some ratios of MUFA-PCs to SFA-PCs or LPCs [PC(36:1)/PC(36:0) and PC(36:1)/LPC(18:0)] were higher in the cancerous areas than the references. The high expression of SCD1 in the cancerous areas was indicative that this enzyme partially mediates the production of MUFA-PCs that were observed in these areas. The analysis of the relative amount of MUFA-PC [PC(34:1) compared to PC(34:0)] through the differences in ER expression suggested the importance of other factors that regulate lipid composition.

Supporting Information

Figure S1 Samples after IMS analysis were severely damaged and closely resembled the adjacent tissue sections microscopically. (a) Adjacent tissue sections that were used for counter staining with hematoxylin and eosin (HE). (b) HE stained samples after IMS analysis.
(TIF)

Figure S2 Comparison of MUFA-PCs to SFA-PCs ratios between cancerous and reference areas on same tissue sections. (a) Plot of the ratios of PC(32:1)+K to PC(32:0)+K. (b) Plot of the ratios of PC(34:1)+K to PC(34:0)+K. (c) Plot of the ratios of PC(36:1)+K to PC(36:0)+K.
(TIFF)

Figure S3 Plot of SCD1 intensity and the MUFA-PCs/SFA-PCs ratio. The values from the subjects were plotted as SCD1 intensity on the x-axis and the MUFA-PCs/SFA-PCs ratio on the y-axis (a, b). A table shows the frequency of the subjects involved in each quadrant divided by the borderlines (a; p = 9.68E-03). The threshold with which bias in the frequencies in the quadrants were proven was not discovered for these molecules. The threshold and the frequency on PCs with 32 acyl carbons were presented since the examination showed relatively low p value.
(TIFF)

Figure S4 Comparison MUFA-PCs to LPCs ratios between cancerous and reference areas on same tissue sections. (a) Plot of the ratios of PC(32:1)+K to LPC(14:0)+K. (b) Plot of the ratios of PC(34:1)+K to LPC(16:0)+K. (c) Plot of the ratios of PC(36:1)+K to LPC(18:0)+K.
(TIFF)

Acknowledgments

We are grateful to the members of Division of Pathology of the Hamamatsu University School of Medicine Hospital for their kind assistance, Yayoi Kawabata and Naomi Suzuki in Department of Laboratory for Histological and Morphological Research, and Koji Ikegami, Noritaka Masaki, Kenji Ohata, Kensuke Goto, and Tsukasa Takahashi in the Department of Cell Biology and Anatomy of the Hamamatsu University School of Medicine for their useful advice.

Author Contributions

Conceived and designed the experiments: YI MW TN YM MS NS. Performed the experiments: YI MW TH TN YM HT TS. Analyzed the data: YI MW TH TN YM MS. Contributed reagents/materials/analysis tools: YI MW TH TN YM HT TS KK RM YH HO MS NS. Wrote the paper: YI MW TH KK MS.

References

1. Jemal A, Bray F, Center MM, Ferlay J, Ward E, et al. (2011) Global cancer statistics. CA Cancer J Clin 61: 69–90.
2. Menendez JA, Lupu R (2007) Fatty acid synthase and the lipogenic phenotype in cancer pathogenesis. Nat Rev Cancer 7: 763–777.
3. Blancato J, Singh B, Liu A, Liao DJ, Dickson RB (2004) Correlation of amplification and overexpression of the c-myc oncogene in high-grade breast cancer: FISH, in situ hybridisation and immunohistochemical analyses. Br J Cancer 90: 1612–1619.
4. Ekroos K, Ejsing CS, Bahr U, Karas M, Simons K, et al. (2003) Charting molecular composition of phosphatidylcholines by fatty acid scanning and ion trap MS3 fragmentation. J Lipid Res 44: 2181–2192.
5. Katz-Brull R, Seger D, Rivenson-Segal D, Rushkin E, Degani H (2002) Metabolic markers of breast cancer: enhanced choline metabolism and reduced choline-ether-phospholipid synthesis. Cancer Res 62: 1966–1970.
6. Podo F, Saradanelli F, Iorio E, Canese R, Carpinelli G, et al. (2007) Abnoramal Choline Phospholipid Metabolism in Breast and Ovary Cancer: Molecular Bases for Noninvasive Imgaging Approaches. Current Medical Imgaging Reviews 3: 123–137.
7. Glunde K, Jie C, Bhujwalla ZM (2004) Molecular causes of the aberrant choline phospholipid metabolism in breast cancer. Cancer Res 64: 4270–4276.

8. Bougnoux P, Chajes V, Lanson M, Hacene K, Body G, et al. (1992) Prognostic significance of tumor phosphatidylcholine stearic acid level in breast carcinoma. Breast Cancer Res Treat 20: 185–194.
9. Hilvo M, Denkert C, Lehtinen L, Muller B, Brockmoller S, et al. (2011) Novel Theranostic Opportunities Offered by Characterization of Altered Membrane Lipid Metabolism in Breast Cancer Progression. Cancer Research 71: 3236–3245.
10. Cornett DS, Reyzer ML, Chaurand P, Caprioli RM (2007) MALDI imaging mass spectrometry: molecular snapshots of biochemical systems. Nat Methods 4: 828–833.
11. Koizumi S, Hayasaka T, Goto-Inoue N, Doi K, Setou M, et al. (2012) Imaging mass spectrometry evaluation of the effects of various irrigation fluids in a rat model of postoperative cerebral edema. World Neurosurg 77: 153–159.
12. Chansela P, Goto-Inoue N, Zaima N, Hayasaka T, Sroyraya M, et al. (2012) Composition and localization of lipids in Penaeus merguiensis ovaries during the ovarian maturation cycle as revealed by imaging mass spectrometry. PLoS ONE 7: e33154.
13. Sugiura Y, Zaima N, Setou M, Ito S, Yao I (2012) Visualization of acetylcholine distribution in central nervous system tissue sections by tandem imaging mass spectrometry. Anal Bioanal Chem 403: 1851–1861.
14. Ntambi JM (1999) Regulation of stearoyl-CoA desaturase by polyunsaturated fatty acids and cholesterol. J Lipid Res 40: 1549–1558.
15. Scaglia N, Caviglia JM, Igal RA (2005) High stearoyl-CoA desaturase protein and activity levels in simian virus 40 transformed-human lung fibroblasts. Biochim Biophys Acta 1687: 141–151.
16. Mauvoisin D, Mounier C (2011) Hormonal and nutritional regulation of SCD1 gene expression. Biochimie 93: 78–86.
17. Luyimbazi D, Akcakanat A, McAuliffe PF, Zhang L, Singh G, et al. (2010) Rapamycin regulates stearoyl CoA desaturase 1 expression in breast cancer. Mol Cancer Ther 9: 2770–2784.
18. Holder AM, Gonzalez-Angulo AM, Chen H, Akcakanat A, Do KA, et al. (2013) High stearoyl-CoA desaturase 1 expression is associated with shorter survival in breast cancer patients. Breast Cancer Res Treat 137: 319–327.
19. Roongta UV, Pabalan JG, Wang X, Ryseck RP, Fargnoli J, et al. (2011) Cancer cell dependence on unsaturated fatty acids implicates stearoyl-CoA desaturase as a target for cancer therapy. Mol Cancer Res 9: 1551–1561.
20. Wolff AC, Hammond ME, Schwartz JN, Hagerty KL, Allred DC, et al. (2007) American Society of Clinical Oncology/College of American Pathologists guideline recommendations for human epidermal growth factor receptor 2 testing in breast cancer. Arch Pathol Lab Med 131: 18–43.
21. Nishimura R, Osako T, Okumura Y, Hayashi M, Toyozumi Y, et al. (2010) Ki-67 as a prognostic marker according to breast cancer subtype and a predictor of recurrence time in primary breast cancer. Exp Ther Med 1: 747–754.
22. Tavassoeli FA, Devilee P (2003) Pathology and Genetics of Tumours of the Breast and Female Genital Organs; Tavassoeli FA, Devilee P, editors: IARCPress.
23. Hayasaka T, Goto-Inoue N, Ushijima M, Yao I, Yuba-Kubo A, et al. (2011) Development of imaging mass spectrometry (IMS) dataset extractor software, IMS convolution. Anal Bioanal Chem 401: 183–193.
24. Hayasaka T, Goto-Inoue N, Zaima N, Kimura Y, Setou M (2009) Organ-specific distributions of lysophosphatidylcholine and triacylglycerol in mouse embryo. Lipids 44: 837–848.
25. Shrivas K, Hayasaka T, Goto-Inoue N, Sugiura Y, Zaima N, et al. (2010) Ionic Matrix for Enhanced MALDI Imaging Mass Spectrometry for Identification of Phospholipids in Mouse Liver and Cerebellum Tissue Sections. Anal Chem 82: 8800–8806.
26. Arita M (2012) Biological importance of fatty acids: from quantity and quality. Experimental Medicine 30: 406–411.
27. Moore S, Knudsen B, True LD, Hawley S, Etzioni R, et al. (2005) Loss of stearoyl-CoA desaturase expression is a frequent event in prostate carcinoma. International Journal of Cancer 114: 563–571.
28. Hilvo M, Denkert C, Lehtinen L, Muller B, Brockmoller S, et al. (2011) Novel theranostic opportunities offered by characterization of altered membrane lipid metabolism in breast cancer progression. Cancer Res 71: 3236–3245.
29. Scaglia N, Chisholm JW, Igal RA (2009) Inhibition of StearoylCoA Desaturase-1 Inactivates Acetyl-CoA Carboxylase and Impairs Proliferation in Cancer Cells: Role of AMPK. PLoS ONE 4: e6812.
30. Hishikawa D, Shindou H, Kobayashi S, Nakanishi H, Taguchi R, et al. (2008) Discovery of a lysophospholipid acyltransferase family essential for membrane asymmetry and diversity. Proc Natl Acad Sci U S A 105: 2830–2835.
31. Iorio E, Ricci A, Bagnoli M, Pisanu ME, Castellano G, et al. (2010) Activation of phosphatidylcholine cycle enzymes in human epithelial ovarian cancer cells. Cancer Res 70: 2126–2135.
32. Chen JE, Smith AG (2012) A look at diacylglycerol acyltransferases (DGATs) in algae. J Biotechnol 162: 28–39.
33. Sorlie T, Tibshirani R, Parker J, Hastie T, Marron JS, et al. (2003) Repeated observation of breast tumor subtypes in independent gene expression data sets. Proc Natl Acad Sci U S A 100: 8418–8423.
34. Scholzen T, Gerdes J (2000) The Ki-67 protein: from the known and the unknown. J Cell Physiol 182: 311–322.
35. Wolff AC, Hammond ME, Schwartz JN, Hagerty KL, Allred DC, et al. (2007) American Society of Clinical Oncology/College of American Pathologists guideline recommendations for human epidermal growth factor receptor 2 testing in breast cancer. J Clin Oncol 25: 118–145.
36. Hammond ME, Hayes DF, Dowsett M, Allred DC, Hagerty KL, et al. (2010) American Society of Clinical Oncology/College Of American Pathologists guideline recommendations for immunohistochemical testing of estrogen and progesterone receptors in breast cancer. J Clin Oncol 28: 2784–2795.
37. Kallioniemi OP, Kallioniemi A, Kurisu W, Thor A, Chen LC, et al. (1992) ERBB2 amplification in breast cancer analyzed by fluorescence in situ hybridization. Proc Natl Acad Sci U S A 89: 5321–5325.
38. Espinosa de los Monteros A, Hellmen E, Ramirez GA, Herraez P, Rodriguez F, et al. (2003) Lipid-rich carcinomas of the mammary gland in seven dogs: clinicopathologic and immunohistochemical features. Vet Pathol 40: 718–723.
39. Shindou H, Hishikawa D, Harayama T, Yuki K, Shimizu T (2009) Recent progress on acyl CoA: lysophospholipid acyltransferase research. J Lipid Res 50 Suppl: S46–51.
40. Miyazaki M, Kim HJ, Man WC, Ntambi JM (2001) Oleoyl-CoA is the major de novo product of stearoyl-CoA desaturase 1 gene isoform and substrate for the biosynthesis of the Harderian gland 1-alkyl-2,3-diacylglycerol. J Biol Chem 276: 39455–39461.
41. Zhao Y, Chen YQ, Bonacci TM, Bredt DS, Li S, et al. (2008) Identification and characterization of a major liver lysophosphatidylcholine acyltransferase. J Biol Chem 283: 8258–8265.
42. EMBL-EBI Available: http://www.ebi.ac.uk/gxa/experiment/E-TABM-276/ENSG00000111684/test_result Accessed November 27 2012.
43. Cheng AS, Culhane AC, Chan MW, Venkataramu CR, Ehrich M, et al. (2008) Epithelial progeny of estrogen-exposed breast progenitor cells display a cancer-like methylome. Cancer Res 68: 1786–1796.
44. Hishikawa D, Shindou H, Kobayashi S, Nakanishi H, Taguchi R, et al. (2008) Discovery of a lysophospholipid acyltransferase family essential for membrane asymmetry and diversity. Proceedings of the National Academy of Sciences 105: 2830–2835.
45. Yoon S, Lee MY, Park SW, Moon JS, Koh YK, et al. (2007) Up-regulation of acetyl-CoA carboxylase alpha and fatty acid synthase by human epidermal growth factor receptor 2 at the translational level in breast cancer cells. J Biol Chem 282: 26122–26131.
46. Sutphen R, Xu Y, Wilbanks GD, Fiorica J, Grendys EC, Jr., et al. (2004) Lysophospholipids are potential biomarkers of ovarian cancer. Cancer Epidemiol Biomarkers Prev 13: 1185–1191.
47. Chughtai K, Jiang L, Greenwood TR, Glunde K, Heeren RM (2013) Mass spectrometry images acylcarnitines, phosphatidylcholines, and sphingomyelin in MDA-MB-231 breast tumor models. J Lipid Res 54: 333–344.
48. Rockett BD, Franklin A, Harris M, Teague H, Rockett A, et al. (2011) Membrane raft organization is more sensitive to disruption by (n-3) PUFA than nonraft organization in EL4 and B cells. J Nutr 141: 1041–1048.
49. Chenais B, Blanckaert V (2012) The janus face of lipids in human breast cancer: how polyunsaturated Fatty acids affect tumor cell hallmarks. Int J Breast Cancer 2012: 712536.
50. Al-Ejeh F, Smart CE, Morrison BJ, Chenevix-Trench G, Lopez JA, et al. (2011) Breast cancer stem cells: treatment resistance and therapeutic opportunities. Carcinogenesis 32: 650–658.
51. Opekarova M, Tanner W (2003) Specific lipid requirements of membrane proteins–a putative bottleneck in heterologous expression. Biochim Biophys Acta 1610: 11–22.
52. Stingl J, Caldas C (2007) Molecular heterogeneity of breast carcinomas and the cancer stem cell hypothesis. Nat Rev Cancer 7: 791–799.
53. Shrivas K, Hayasaka T, Sugiura Y, Setou M (2011) Method for simultaneous imaging of endogenous low molecular weight metabolites in mouse brain using TiO2 nanoparticles in nanoparticle-assisted laser desorption/ionization-imaging mass spectrometry. Anal Chem 83: 7283–7289.
54. Waki ML, Onoue K, Takahashi T, Goto K, Saito Y, et al. (2011) Investigation by imaging mass spectrometry of biomarker candidates for aging in the hair cortex. PLoS ONE 6: e26721.

Research Article

EASL EUROPEAN ASSOCIATION FOR THE STUDY OF THE LIVER | JOURNAL OF HEPATOLOGY

Lysophosphatidylcholine acyltransferase 1 altered phospholipid composition and regulated hepatoma progression

Yoshifumi Morita[1,2], Takanori Sakaguchi[1], Koji Ikegami[2], Naoko Goto-Inoue[2], Takahiro Hayasaka[2], Vu Thi Hang[2], Hiroki Tanaka[1], Takashi Harada[1], Yasushi Shibasaki[1], Atsushi Suzuki[1], Kazuhiko Fukumoto[1], Keisuke Inaba[1], Makoto Murakami[3], Mitsutoshi Setou[2,*], Hiroyuki Konno[1]

[1]*Second Department of Surgery, Hamamatsu University School of Medicine, Japan;* [2]*Department of Cell Biology and Anatomy, Hamamatsu University School of Medicine, Japan;* [3]*Lipid Metabolism Project, Department of Advanced Science for Biomolecules, Tokyo Metropolitan Institute of Medical Science, Japan*

Background & Aims: Several lipid synthesis pathways play important roles in the development and progression of hepatocellular carcinoma (HCC), although the precise molecular mechanisms remain to be elucidated. Here, we show the relationship between HCC progression and alteration of phospholipid composition regulated by lysophosphatidylcholine acyltransferase (LPCAT).

Methods: Molecular lipidomic screening was performed by imaging mass spectrometry (IMS) in 37 resected HCC specimens. RT-PCR and Western blotting were carried out to examine the mRNA and protein levels of LPCATs, which catalyze the conversion of lysophosphatidylcholine (LPC) into phosphatidylcholine (PC) and have substrate specificity for some kinds of fatty acids. We examined the effect of LPCAT1 overexpression or knockdown on cell proliferation, migration, and invasion in HCC cell lines.

Results: IMS revealed the increase of PC species with palmitoleic acid or oleic acid at the *sn-2*-position and the reduction of LPC with palmitic acid at the *sn-1*-position in HCC tissues. mRNA and protein of LPCAT1, responsible for LPC to PC conversion, were more abundant in HCCs than in the surrounding parenchyma. In cell line experiments, LPCAT1 overexpression enriched PCs observed in IMS and promoted cell proliferation, migration, and invasion. LPCAT1 knockdown did *viceversa*.

Conclusions: Enrichment or depletion of some specific PCs, was found in HCC by IMS. Alteration of phospholipid composition in HCC would affect tumor character. LPCAT1 modulates phospholipid composition to create favorable conditions to HCC cells. LPCAT1 is a potent target molecule to inhibit HCC progression.

Keywords: Cancer lipidomics; Imaging mass spectrometry; LPCAT1; Hepatocellular carcinoma.

Received 4 May 2012; received in revised form 8 February 2013; accepted 18 February 2013

* Corresponding author. Address: Department of Cell Biology and Anatomy, Hamamatsu University School of Medicine, 1-20-1 Handayama, Higashi-ku, Hamamatsu 431-3192, Japan. Tel./fax: +81 53 435 2292.

E-mail address: setou@hama-med.ac.jp (M. Setou).

Abbreviations: HCC, hepatocellular carcinoma; NAFLD, non-alcoholic fatty liver disease; IMS, imaging mass spectrometry; MALDI, matrix-assisted laser desorption/ionization; LPCAT, lysophosphatidylcholine acyltransferase; PCA, principal component analysis; $cPLA_2\alpha$, cytosolic phospholipase $A_2\alpha$; $iPLA_2\beta$, Ca^{2+}-independent phospholipase $A_2\beta$; LPC, lysophosphatidylcholine; PC, phosphatidylcholine; DPPC, dipalmitoyl phosphatidylcholine; PAF, platelet activating factor.

Introduction

Hepatocellular carcinoma (HCC) is the seventh most frequently diagnosed cancer and the fourth most frequent cause of cancer-related death in the world [1]. The frequency of HCC has increased in the United States and in European and Asian countries [2]. In addition to HBV, HCV, alcohol, and aflatoxin, non-alcoholic fatty liver disease (NAFLD) has drawn increasing attention as a risk factor of HCC. NAFLD is the most common form of chronic liver disease in developed countries. Alteration of the lipogenic pathway plays an important role in the pathogenesis of NAFLD and also in HCC carcinogenesis and its progression [3].

In recent years, imaging mass spectrometry (IMS) using matrix-assisted laser desorption/ionization (MALDI) has emerged and developed dramatically in the field of proteomics and metabolomics [4,5]. MALDI-IMS can clarify the distribution of lipid molecules, directly from heterogeneous tissue samples, by determining the differences in the mass-to-charge ratios (*m/z*). Furthermore, tandem mass spectrometry (MS/MS analysis), which generates the fragment ion spectrum by spraying additional collision gas, enables the identification of the molecules in tissues by providing detailed information on their structures. IMS has been used to classify tumor grade or to investigate new biomarkers in cancer proteomics [6,7]. At present, there are only limited reports on molecular proteomics of HCC using IMS [8,9].

In this study, we performed IMS using HCC tissue samples as molecular lipidomic screening and revealed the alteration of phospholipid composition caused by overexpressed LPCAT1. We further investigated the role of LPCAT1 in HCC progression and

Please cite this article in press as: Morita Y et al. Lysophosphatidylcholine acyltransferase 1 altered phospholipid composition and regulated hepatoma progression. J Hepatol (2013), http://dx.doi.org/10.1016/j.jhep.2013.02.030

Research Article

elucidated that LPCAT1 increased cell proliferation and invasion, using hepatoma cell lines.

Materials and methods

Clinical specimens

Human HCC tissues, including a boundary region, were excised from resected specimens provided by our institute. A total of 37 samples were obtained from surgical specimens. The clinicopathological characteristics are listed in Table 1. Samples were snap-frozen in liquid nitrogen and stored at −80 °C. The study protocol was approved by the ethical committee of our institute, and all the patients gave informed consent for the procedures.

Imaging mass spectrometry using clinical specimens

The frozen tissues were sliced into 10-μm-thick serial sections; furthermore, for H&E staining, they were sliced into 5-μm-thick sections, using a cryostat (CM1950, Leica Microsystems, Germany). The samples for IMS were put onto indium-tin-oxide-coated glass slides (Bruker Daltonics, Germany) and dried at room temperature. The matrix solution was prepared by dissolving 50 mg/ml 2,5-dihydroxybenzoic acid (Bruker Daltonics) in 70% methanol. A thin matrix layer was applied to the surface of the plates as described previously [10]. Mass spectra were acquired using Ultraflex II (Bruker Daltonics). In this analysis, we collected signals between *m/z* 400 and 1000 in positive ion mode. The mechanical resolution was 100 μm × 100 μm. The number of laser irradiations was 200 shots in each spot. Image reconstruction was performed using FlexImaging 2.1 software (Bruker Daltonics). The 100 most intense peaks between HCC and normal parenchyma in a single analysis were compared by principal component analysis (PCA) utilizing ClinProTool 2.2 software (Bruker Daltonics). An alignment of mass spectra from different samples was performed using SpecAlign software (http://physchem.ox.ac.uk/~jwong/specalign/). The peak intensity value of the spectra was normalized by dividing by the total ion current, as previously described [11].

Table 1. Patients clinicopathological features.

Sex	
Male	30
Female	7
Age	68 (45-80)
Etiology	
HBV	7
HCV	25
NBNC*	5
Tumor size (maximum diameter), cm	3.0 (1.3-10)
Tumor number	2 (1-7)
Vascular invasion	
Positive	11
Negative	26
Stage (UICC)	
I	15
II	19
IIIA	3
Differentiation	
Well	11
Moderate	24
Poor	1
α-fetoprotein, ng/ml	337 (2-8989)
PIVKA-II, mAU/ml	419 (15-8830)

NBNC, non-B, non-C hepatitis.
*NBNC contains no alcohol addict.

Identification of biomolecules

Tandem mass spectrometry was performed using QSTAR Elite (Applied Biosystems Inc., Foster City, CA), a hybrid quadrupole/time-of-flight mass spectrometer equipped with an orthogonal MALDI source and a pulsed Nd:YAG. The MS/MS analysis was performed directly on the tissue sections. The data acquisition conditions (i.e., the laser power, collision energy, and the number of laser irradiations) were adjusted to obtain good-quality mass spectra with high intensity and signal-to-noise ratios (S/N) in the fragmented peaks. The MS/MS data were assigned using Nature Lipidomics Gateway (http://www.lipidmaps.org/).

Semi-quantitative RT-PCR

Total RNA was extracted using RNeasy mini kit (QIAGEN, Valencia, CA) for tissue samples and Sepasol I (Nakalai Tesque, Japan) for cells, respectively. The extracted RNAs from tissue samples and cells were reverse-transcribed with SuperScript III (Invitrogen, Carlsbad, CA) and ReverTra Ace (TOYOBO LIFE SCIENCE, Japan), respectively. Each single-stranded cDNA of LPCATs and *GAPDH* was amplified on a GeneAmp PCR System 9700 (Applied Biosystems Inc.). PCR primer sequences and reaction conditions are listed in Supplementary Table 1. The PCR bands were visualized using gel documentation system Printgraph AE6932CP-4 (ATTO, Tokyo, Japan). The signal intensity of each band was digitized as a cumulative density of band area. This digitizing of band signal was easily done with a macro command available in Scion image software version 4.0.3.2 (Scion Corporation, Frederick, MD). Signal intensities of LPCATs of each sample were normalized to those of *GAPDH* of the same sample. We confirmed that *GAPDH* was able to be used as a reference as the difference of *GAPDH* signal between cancer and non-cancer was less than 1.2 and not statistically significant. The data were presented as the ratio of LPCATs and *GAPDH*. We loaded all the samples into one gel for quantitative comparison.

Western blotting

A rabbit polyclonal anti-LPCAT1 antibody (Protein Tech Group, Inc., Chicago, IL), rabbit polyclonal anti-LPCAT4 antibody (Protein Tech Group, Inc.), rabbit monoclonal anti-cytosolic phospholipase $A_2\alpha$ ($cPLA_2\alpha$) antibody (Cell Signaling Technology, Inc., Beverly, MA), rabbit polyclonal anti-Ca^{2+}-independent phospholipase A_2 β ($iPLA_2\beta$) antibody (Abcam, UK), mouse monoclonal anti-GAPDH antibody (Millipore Corporate, Billerica, MA), and mouse monoclonal anti-FLAG M2 antibody (Agilent Technology, Santa Clara, CA) were used. The immunoreactive bands were visualized using ECL plus Western Blotting Detection Reagents (GE Healthcare, UK) and an Imaging Reader LAS-3000 mini (FUJIFILM, Japan). We checked the band of LPCAT1 and 4 detected with knockdown samples. We observed that in knockdown samples, the specific band was absent. The evaluation was carried out by quantifying the signal intensity of visible bands with Scion image software.

Cell lines

HCC cell lines HuH7 and HepG2 cells were purchased from Human Science Research Resources Bank (Japan). They were cultured under Dulbecco's modified Eagle's medium (Invitrogen) with 10% fetal bovine serum, 100 U penicillin, and 0.1 mg/ml streptomycin at 37 °C in 5% CO_2.

Small interfering RNA inhibition assay

To knock down endogenous LPCAT1 expression in HuH7 and HepG2 cells, we used Stealth RNAi (Invitrogen). We used Stealth RNAi Negative Control Medium GC Duplex #2 (Invitrogen) as a negative control. HuH7 and HepG2 cells were seeded and transfected with Lipofectamine 2000 (Invitrogen), according to the manufacturer's instructions. The HuH7 and HepG2 cells were harvested 4 days and 3 days after transfection, respectively.

Expression plasmids

The full-length cDNA encoding human *LPCAT1* was purchased from DNAFORM (Japan). The full-length cDNA was amplified using the following primers: sense, 5′-gggGGATCCatgaggctgcggggatgcg and antisense, 3′-gggGAATTCctaatccagcttcttgcgaaca. The amplified fragments were cloned into pCMV-Tag2 vector (Agilent Technologies, Inc.) at *Bam*HI-*Eco*RI sites. All DNA sequences were verified

Please cite this article in press as: Morita Y et al. Lysophosphatidylcholine acyltransferase 1 altered phospholipid composition and regulated hepatoma progression. J Hepatol (2013), http://dx.doi.org/10.1016/j.jhep.2013.02.030

using genetic analyzer ABI PRISM® 3100 (Applied Biosystems Inc.). HuH7 and HepG2 cells were harvested 48 h after transfection with Lipofectamine 2000. pCMV-Tag3c vector (Agilent Technologies, Inc.) was used as a negative control.

Imaging mass spectrometry using carcinoma cell lines

1×10^5 HuH7 and 1.5×10^5 HepG2 cells after transfection were seeded on the ITO slide glass with 8 well FlexiPERM (Greiner Bio-one, Germany) and incubated at 37 °C in 5% CO_2 for 12 h. Then, the medium was removed and the wells were washed three times using 0.1 M phosphate buffer. After drying, a thin matrix layer was applied using matrix sublimation equipment RK27-4069 (Shimadzu Corp, Japan) according to the manufacturer's protocol. Mass spectra were acquired using Ultraflex II. The raster width was 50 μm × 50 μm and the number of laser irradiations was 200 shots in each spot. The 100 most intense peaks acquired from 1500 irradiation points were compared using ClinProTool 2.2 software. The cell confluency was evaluated by the 200× magnified images with Scion image software.

Cell proliferation assay

In knockdown experiments, 2×10^3 HuH7 cells and 4×10^3 HepG2 cells were plated in 96-well plates. Cell proliferation was measured at 3 and 5 days after completion of knockdown. In overexpression experiments, 4×10^3 cells were plated in 96-well plates. Cell proliferation was measured at 2 and 4 days after transfection. MTT Cell Growth Assay Kit (Millipore Corporation) was used according to manufacturer's instructions. The absorbance for live cells was measured with Synergy HT Multi-Mode Microplate Reader (BioTek, Winooski, VT). Analysis was performed on 12 independent wells for each condition and the experiments were repeated three times.

Cell migration and invasion assay

The *in vitro* migration and invasion activities of cells were evaluated using Cell Culture Insert and Matrigel invasion chamber (Becton Dickinson, Bedford, MA) separated by an 8 mm-pore filter membrane. 4×10^4 HuH7 cells and 1×10^5 HepG2 cells in 0.5 ml of serum-free medium were seeded on the upper chamber, and the lower chamber was loaded with 0.75 ml medium with 10% fetal bovine serum. After cultivation for 48 h, cells passed through the membrane were stained with Diff Quik solution (International Reagents, Japan) and counted under an optical microscope, in five randomly selected 100× magnification fields for one membrane. We used three wells for each condition in one experiment.

Statistical analysis

Statistical analyses were performed with Stat View software (version 5.0; Abacus Concepts, Inc., Berkeley, CA) and ClinProTool 2.2 software. Wilcoxon signed-rank test was used for comparison of the measurable variants of two groups. Analysis of variance and Fisher's protected least significant difference tests were performed as *post hoc* tests for the comparison of measurable variants of three or more groups. $p < 0.05$ was defined as statistically significant.

Results

IMS revealed the alteration of phospholipid composition in HCC

We performed IMS of the boundary area containing both cancer and normal liver parenchyma in the HCC tissue sample (Fig. 1A). Mass spectra acquired from cancer tissue seemed to be different from those of the normal liver parenchyma at various *m/z* values (Supplementary Fig. 1A). Unsupervised multivariate analysis, PCA, was performed to identify the different peaks between cancer region and normal region. PCA revealed that the spectra acquired from HCC were quite different from those of the non-cancerous region on the first principal component (Supplementary Fig. 1B). The corresponding loading plot showed the influence of the *m/z* value on the respective principal components (Supplementary Fig. 1C). Subsequently, we performed MS/MS analyses of the detected signals and identified 19 biomolecules with the exception of isotopic data (Table 2). They were composed of 2 lysophosphatidylcholines (LPCs) (No. 1 and 2 in Supplementary Fig. 1C), 13 phosphatidylcholines (PCs) (No. 5–17), 2 triglycerides (No. 18 and 19), 1 sphingomyelin (No. 4), and 1 Heme (No. 3). In particular, *m/z* 770.4 (PC (16:0/16:1), No. 5 in Supplementary Fig. 1C) was one of the most influential peaks on the first principle component. Actually, PC (16:0/16:1) was abundant in the cancerous region from the IMS result (Fig. 1B, middle panel). Meanwhile, LPC (16:0) was scarce in the cancerous region (Fig. 1B, left panel). We normalized the

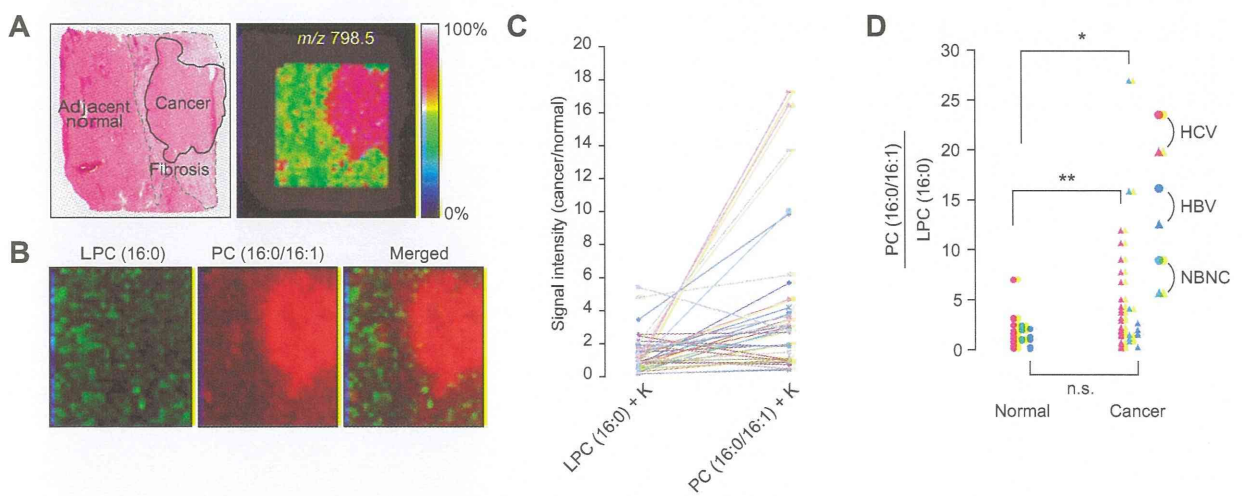

Fig. 1. Imaging mass spectrometry using HCC tissue sample and quantitative analyses of signal intensities in PC and LPC species. (A) Representative histologic finding (H&E staining) and its IMS image at *m/z* 798.5 of HCC tissue sample are shown in the left and right panel, respectively. (B) Reconstructed images acquired from IMS. LPC (16:0): green, PC (16:0/16:1): red, and the merged image are shown. (C) Cancer-to-normal ratios in LPC (16:0) and PC (16:0/16:1) in 37 HCC tissue samples. (D) PC (16:0/16:1)-to-LPC (16:0) ratios in 37 HCC tissue samples. *$p < 0.05$; **$p < 0.01$; n.s., not significant.

Please cite this article in press as: Morita Y et al. Lysophosphatidylcholine acyltransferase 1 altered phospholipid composition and regulated hepatoma progression. J Hepatol (2013), http://dx.doi.org/10.1016/j.jhep.2013.02.030

Research Article

Table 2. The list of biomolecules identified by MS/MS analysis.

No.	Common name	Formula	Calculated mass	Observed mass	Delta	Adduct
1	LysoPC (16:0)	C24H50NO7P	534.2956	534.2930	0.0026	M + K
2	LysoPC (18:0)	C26H54NO7P	562.3269	562.3111	0.0158	M + K
3	Heme B	C34H32O4N4Fe	616.1773	616.1737	0.0036	M + H
4	SM (d18:0/16:1)	C39H79N2O6P	725.5568	725.5499	0.0069	M + Na
5	PC (16:0/16:1)	C40H78NO8P	770.5096	770.4028	0.1068	M + K
6	PC (18:1/18:1)	C44H84NO8P	786.5934	786.4791	0.1143	M + H
7	PC (16:0/18:2)	C42H80NO8P	796.5252	796.5214	0.0038	M + K
8	PC (16:0/18:1)	C42H82NO8P	798.5409	798.5348	0.0061	M + K
9	PC (16:0/20:4)	C44H80NO8P	820.5252	820.5219	0.0033	M + K
10	PC (18:1/18:2)	C44H82NO8P	822.5409	822.4802	0.0607	M + K
11	PC (18:0/18:2)	C44H84NO8P	824.5565	824.4588	0.0977	M + K
12	PC (18:0/18:1)	C44H86NO8P	826.5722	826.4737	0.0985	M + K
13	PC (18:2/20:4)	C46H80NO8P	828.5513	828.4791	0.0722	M + Na
14	PC (18:1/20:4)	C46H82NO8P	846.5409	846.4841	0.0568	M + K
15	PC (18:0/20:4)	C46H84NO8P	848.5565	848.5053	0.0512	M + K
16	PC (18:1/22:6)	C48H82NO8P	870.5409	870.4749	0.0660	M + K
17	PC (18:0/22:6)	C48H84NO8P	872.5565	872.4901	0.0664	M + K
18	TG (16:0/18:1/18:2)	C55H100O6	895.7151	895.7016	0.0135	M + K
19	TG (52/2)	C55H102O6	897.7307	897.7282	0.0025	M + K

Each No. is identical to the number in PCA (Supplementary Fig. 1C).
The common name, formula, and calculated mass were acquired from Nature Lipidomics Gateway and HMBD.
Delta means the difference between calculated mass and observed mass.
Adduct means adductive ions such as H, Na, and K to original molecules (M).

spectra acquired from 37 samples using total ion current with SpecAlign software, and quantified the signal intensity of each biomolecule. The signal intensity of PC (16:0/16:1) was significantly higher in the cancerous region than in the normal region (Fig. 1C). Furthermore, the calculated PC-to-LPC ratios, such as PC (16:0/16:1)/LPC (16:0) in the HCV-related and non-virus-related cancer region, were significantly higher than those in the normal region. PC (16:0/18:1)/LPC (16:0) and PC (18:0/18:1)/LPC (18:0) in the HCV-related cancer region were significantly higher than those in the normal region (p <0.05, Fig. 1D and Supplementary Fig. 2).

LPCAT1 mRNA and protein are highly expressed in HCC

We hypothesized that the alteration of PC-to-LPC ratios in HCC was caused by the increase of specific PC formation from LPC. The homeostasis of phospholipid composition is mainly balanced by LPCATs and PLA_2s. Initially, we investigated the expression level of four LPCATs, which were responsible for LPC to PC conversion, using the RNA extracted from 18 tissue samples (12 HCV-related, 3 HBV-related, and 3 non-virus-related, Fig. 2A). *LPCAT1* and *LPCAT4*, but not *LPCAT2* and *LPCAT3*, were highly expressed in cancers (*LPCAT1*, p <0.01; *LPCAT4*, p <0.05). We further found the significantly higher expression of LPCAT1 protein in HCC (Fig. 2B, p <0.01). Furthermore, the expression level of LPCAT1 protein correlated well with the signal intensity of PC (16:0/16:1) (Fig. 2C). Meanwhile, the expression level of $cPLA_2\alpha$ and $iPLA_2\beta$, which were the candidates to maintain phospholipid composition [12], were not different between the HCC and normal region (Supplementary Fig. 3).

LPCAT1 knockdown changed the PC composition in hepatoma cell lines

We performed an *in vitro* knockdown experiment to investigate the influence of LPCAT1 on PC compositions using two HCC cell lines, HuH7 and HepG2. Fig. 3 and Supplementary Fig. 4 represent the data obtained from the experiments using HuH7 and HepG2 cells, respectively. In both cell lines, reductions in LPCAT1 mRNA and protein were observed after transfection with *LPCAT1*-targeting siRNA compared with an unsilencing siRNA (Fig. 3A, Supplementary Fig. 4A). We confirmed the reduction of some PCs, such as PC (16:0/16:1), after LPCAT1 knockdown using IMS (Fig. 3B and Supplementary Fig. 4B, left and lower panels) in the comparable condition of confluency (Fig. 3B and Supplementary Fig. 4B, right panel). In HuH7 cells, we could detect the alteration of signal intensity relative to that in the control group in six PC species (Fig. 3C). In HepG2 cells, we could detect the alteration of signal intensity in five PC species (Supplementary Fig. 4C).

LPCAT1 knockdown reduced cell proliferation, migration and invasion

We further investigated the influence of LPCAT1 in cell proliferation. LPCAT1 knockdown (siRNA1 and siRNA3) significantly reduced cell proliferation both 3 and 5 days after completion of knockdown in both HuH7 and HepG2 cells (Table 3). Next, we examined the effect of LPCAT1 knockdown on cell migration and invasion. Both the migration and invasion were significantly inhibited after knockdown of LPCAT1 (Table 4).

Please cite this article in press as: Morita Y et al. Lysophosphatidylcholine acyltransferase 1 altered phospholipid composition and regulated hepatoma progression. J Hepatol (2013), http://dx.doi.org/10.1016/j.jhep.2013.02.030

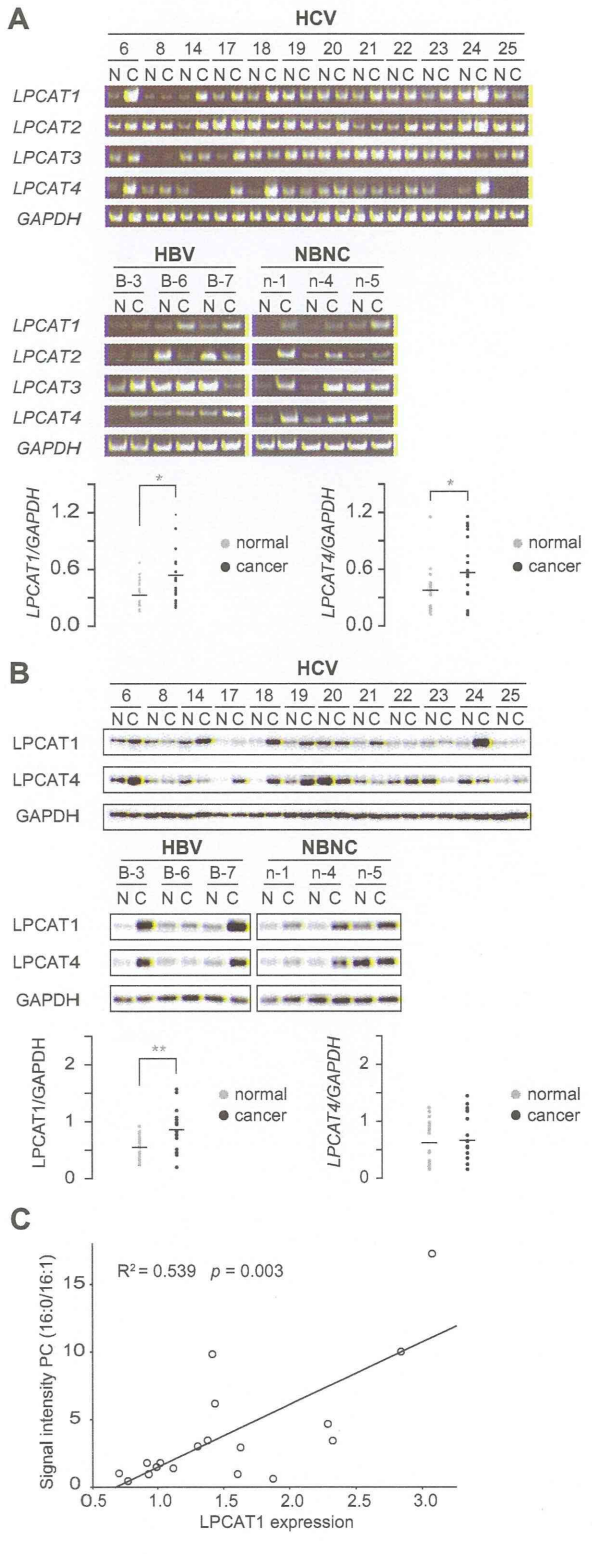

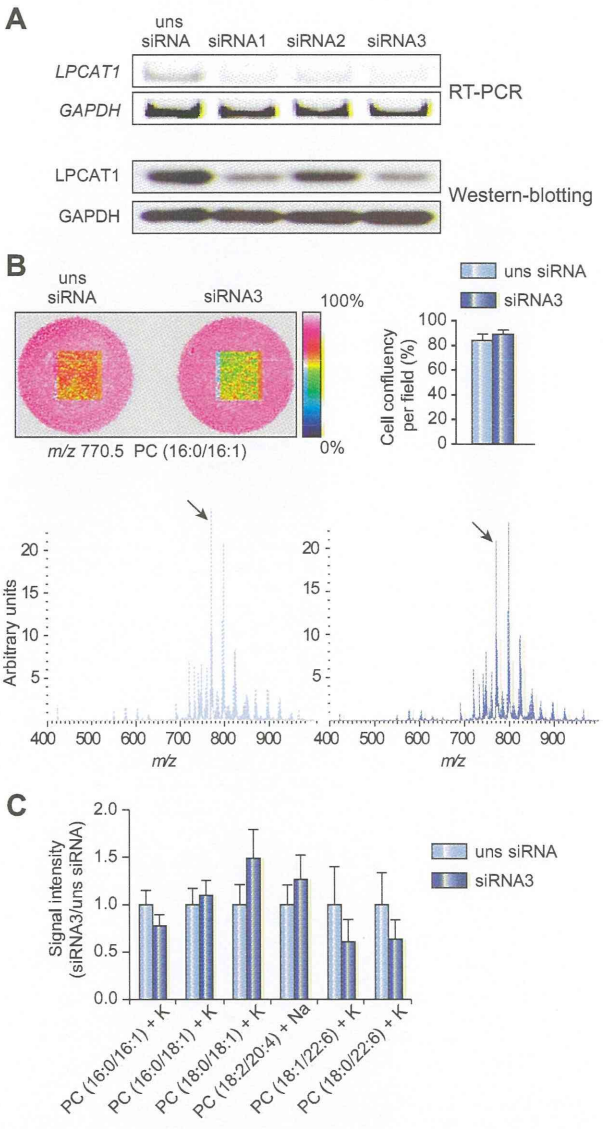

Fig. 3. LPCAT1 knockdown changes PC composition. (A) RT-PCR (upper panel) and Western blotting (lower panel) using HuH7 cells transfected with siRNA to *LPCAT1*, as well as an unsilencing (uns) siRNA. (B) IMS images of PC (16:0/16:1) at *m/z* 770.5 are shown in squares. The color gradient bar indicates the relative intensity. The upper right panel shows the cell confluency for 200× magnified fields. Lower panels show the mass spectra acquired from IMS. The arrows indicate the peaks of PC (16:0/16:1) at *m/z* 770.5. Values are mean ± SD (n = 5). (C) Significantly altered PC species in 3 independent experiments are shown. Values are mean ± SD (n = 1500).

Fig. 2. RT-PCR and Western blotting using HCC tissue extracts. (A) Semiquantitative RT-PCR analyses of *LPCAT1-4* in 12 HCV, 3 HBV, and 3 non-virus-related HCCs. N and C represent adjacent normal parenchyma and cancer tissue, respectively. The experiments were repeated twice. (B) Western blotting analyses of LPCAT1 and LPCAT4 proteins. The experiments were repeated three times. In both panels (A) and (B), lower panels show the densitometric quantification of signal intensities using GAPDH as internal standard. The horizontal line represents the median value (n = 18); $^{*}p < 0.05$; $^{**}p < 0.01$. (C) Correlation between expression level of LPCAT1 protein (*x*-axis) and signal intensity of PC (16:0/16:1) (*y*-axis) is shown.

Please cite this article in press as: Morita Y et al. Lysophosphatidylcholine acyltransferase 1 altered phospholipid composition and regulated hepatoma progression. J Hepatol (2013), http://dx.doi.org/10.1016/j.jhep.2013.02.030

Research Article

Table 3. LPCAT1 knockdown or overexpression affected cell proliferation.

	Cell proliferation (absorbance 570-630 nm)			
	HuH7		HepG2	
	Day 3	Day 5	Day 3	Day 5
Control siRNA				
uns siRNA	0.096 ± 0.011	0.135 ± 0.013	0.409 ± 0.025	0.839 ± 0.043
LPCAT1-siRNA				
siRNA1	0.079 ± 0.008**	0.127 ± 0.010**	0.364 ± 0.021**	0.790 ± 0.097
siRNA3	0.041 ± 0.005**	0.082 ± 0.017**	0.304 ± 0.020**	0.740 ± 0.050**
	Day 2	Day 4	Day 2	Day 4
Control vector				
pCMV-Tag3c	0.266 ± 0.028	0.294 ± 0.042	0.170 ± 0.020	0.226 ± 0.024
LPCAT1-overexpression				
pCMV-Tag2-*LPCAT1*	0.298 ± 0.028**	0.309 ± 0.031	0.182 ± 0.022	0.312 ± 0.029**

Values are mean ± SD (n = 12).
**p <0.01.
uns, unsilencing.

Overexpression of LPCAT1 changed the PC composition in hepatoma cell lines

Next, we generated the CMV-driven mammalian expression vector (pCMV-Tag2-LPCAT1) to investigate the effect of LPCAT1 overexpression on PC compositions. Fig. 4 and Supplementary Fig. 5 represent the data obtained from the experiments using HuH7 and HepG2 cells, respectively. Following expression of this plasmid, a significant increase of LPCAT1 protein was found in Western blotting and immunofluorescent analysis (Fig. 4A and Supplementary Fig. 5A). We confirmed the increase of some PCs, such as PC (16:0/16:1), after LPCAT1 overexpression using IMS (Fig. 4B and Supplementary Fig. 5B, left and lower panels) in comparable conditions of confluency (Fig. 4B and Supplementary Fig. 5B, right panel). In HuH7 cells, we could detect the alteration of signal intensity relative to that in the control group in six PC species (Fig. 4C). In HepG2 cells, we could detect the alteration of signal intensity in seven PC species (Supplementary Fig. 5C).

LPCAT1 overexpression accelerated cell proliferation and invasion

LPCAT1 overexpression significantly increased cell proliferation 2 days after transfection in HuH7 cells. In HepG2 cells, LPCAT1 overexpression significantly increased cell proliferation 4 days after transfection (Table 3). Finally, we examined the effect of LPCAT1 overexpression on cell migration and invasion. The invasion capacity was significantly enhanced after transfection in both HuH7 cells and HepG2 cells (Table 4). On the other hand, the migration ability was not affected in these experiments.

Table 4. LPCAT1 knockdown or overexpression affected cell migration and invasion.

	HuH7	HepG2
Migrated cells per field (cell migration)		
Control siRNA		
uns siRNA	297 ± 119	289 ± 120
LPCAT1-siRNA		
siRNA3	210 ± 78**	132 ± 49**
Control vector		
pCMV-Tag3c	143 ± 51	37 ± 34
LPCAT1-overexpression		
pCMV-Tag2-*LPCAT1*	140 ± 58	42 ± 40
Invaded cells per field (cell invasion)		
Control siRNA		
uns siRNA	102 ± 55	173 ± 130
LPCAT1-siRNA		
siRNA3	22 ± 11**	76 ± 59**
Control vector		
pCMV-Tag3c	48 ± 18	11 ± 11
LPCAT1-overexpression		
pCMV-Tag2-*LPCAT1*	76 ± 48**	22 ± 21**

Values are mean ± SD (n = 15).
**p <0.01.
uns, unsilencing.

Discussion

Aberrant lipid synthesis pathways are thought to be involved in HCC pathophysiology. In this study, we investigated the lipid distribution and composition in clinical HCC samples. IMS revealed that monounsaturated fatty-containing PCs were abundant in HCC. This is in agreement with the literature, which reports an increased ratio of monounsaturated to saturated fatty acids in livers of mice prone to HCC development [13]. Furthermore, palmitoyl acid-containing LPC was scarce in cancerous regions. An additional observation was the paucity of polyunsaturated or highly unsaturated fatty acid-containing PCs in HCC areas (not shown), which concurs with literature reports of omega-3 fatty acids inhibiting the growth of HCC [14]. Taken together, our results suggest that selective changes in the PC and LPC composition promote HCC progression.

Phospholipids are formed from glycerol 3-phosphate by the *de novo* pathway or by remodeling the existing PC species. The *de novo* pathway was originally described by Kennedy and Weiss [15]. Saturated and monounsaturated fatty acids are usually esterified at the *sn-1*-position, whereas unsaturated acyl groups are esterified at the *sn-2*-position. This diversity and asymmetry are not fully explained by the Kennedy pathway. The remodeling

Please cite this article in press as: Morita Y et al. Lysophosphatidylcholine acyltransferase 1 altered phospholipid composition and regulated hepatoma progression. J Hepatol (2013), http://dx.doi.org/10.1016/j.jhep.2013.02.030